Short-term reduction of regional enhancement of atmospheric CO2in China during the first COVID-19 pandemic period

Sojung Sim, Haeyoung Lee, Eunsil Oh, Sumin Kim, Philippe Ciais, Shilong Piao, John Chun Han Lin, Derek V. Mallia, Sepyo Lee, Yeon-Hee Kim, et al.

ENVIRONMENTAL RESEARCH
LETTERS

LETTER • OPEN ACCESS

Short-term reduction of regional enhancement of atmospheric CO_2 in China during the first COVID-19 pandemic period

To cite this article: Sojung Sim *et al* 2022 *Environ. Res. Lett.* **17** 024036

ENVIRONMENTAL RESEARCH
LETTERS

LETTER

Short-term reduction of regional enhancement of atmospheric CO_2 in China during the first COVID-19 pandemic period

Sojung Sim[1], Haeyoung Lee[2], Eunsil Oh[1], Sumin Kim[2], Philippe Ciais[3], Shilong Piao[4], John C Lin[5], Derek V Mallia[5], Sepyo Lee[2], Yeon-Hee Kim[2], Hoonyoung Park[1], Jeongmin Yun[1] and Sujong Jeong[1,*]

[1] Department of Environmental Planning, Graduate School of Environmental Studies, Seoul National University, Seoul 08826, Republic of Korea
[2] Innovative Meteorological Research Department, National Institute of Meteorological Sciences, Jeju 63568, Republic of Korea
[3] Laboratoire des Sciences du Climat et de l'Environment, CEA-CNRS-UVSQ, UMR8212 Gif-sur-Yvette, France
[4] Key Laboratory of Alpine Ecology and Biodiversity, Institute of Tibetan Plateau Research, Chinese Academy of Sciences, Beijing, People's Republic of China
[5] Department of Atmospheric Sciences, University of Utah, Salt Lake City, UT, United States of America
* Author to whom any correspondence should be addressed.

E-mail: sujong@snu.ac.kr

Keywords: COVID-19, lockdown, carbon dioxide, atmospheric reduction, WRF-STILT, China

Supplementary material for this article is available online

OPEN ACCESS

RECEIVED
3 December 2020

REVISED
26 January 2022

ACCEPTED FOR PUBLICATION
31 January 2022

PUBLISHED
14 February 2022

Abstract

Recent studies have reported a 9% decrease in global carbon emissions during the COVID-19 lockdown period; however, its impact on the variation of atmospheric CO_2 level remains under question. Using atmospheric CO_2 observed at Anmyeondo station (AMY) in South Korea, downstream of China, this study examines whether the decrease in China's emissions due to COVID-19 can be detected from the enhancement of CO_2 mole fraction (ΔCO_2) relative to the background value. The Weather Research and Forecasting–Stochastic Time-Inverted Lagrangian Transport model was applied to determine when the observed mole fractions at AMY were affected by air parcels from China. Atmospheric observations at AMY showed up to a −20% (−1.92 ppm) decrease in ΔCO_2 between February and March 2020 compared to the same period in 2018 and 2019, particularly with a −34% (−3.61 ppm) decrease in March. ΔCO, which was analyzed to explore the short-term effect of emission reductions, had a decrease of −43% (−80.66 ppb) during the lockdown in China. Particularly in East China, where emissions are more concentrated than in Northeast China, ΔCO_2 and ΔCO decreased by −44% and −65%, respectively. The $\Delta CO/\Delta CO_2$ ratio (24.8 ppb ppm^{-1}), which is the indicator of emission characteristics, did not show a significant difference before and after the COVID-19 lockdown period ($\alpha = 0.05$), suggesting that this decrease in ΔCO_2 and ΔCO was associated with emission reductions rather than changes in emission sources or combustion efficiency in China. Reduced carbon emissions due to limited human activity resulted in a decrease in the short-term regional enhancement to the observed atmospheric CO_2.

1. Introduction

To prevent the rapid spread of the novel coronavirus disease, COVID-19, Wuhan City imposed a lockdown on 23 January 2020, and preventive measures, such as confinement, school and workplace closures, physical distancing, and social restrictions were implemented throughout China from late January to April 2020. These measures dramatically reduced economic and social activities, and consequently, the emission of carbon dioxide (CO_2) (Lauri Le Quéré *et al* 2020, Liu *et al* 2020, Myllyvirta 2020). A recent study by Le Quéré *et al* (2020) estimated a −2.6% (−242 Mt CO_2) change in CO_2 emission in China from 1 January to 30 April 2020, compared to that in 2019. Similarly, Liu *et al* (2020) discovered a 3.7% reduction (−187.2 Mt CO_2) in China from 1 January to 30 June 2020, with 18.4% and 9.2% reductions in February

and March 2020, respectively, compared to the same period in 2019. Therefore, it is crucial to determine whether the influence of emission reductions in China is strong enough to be detected from atmospheric CO_2 observations because atmospheric CO_2 levels have a direct impact on climate change.

Although the recent lockdown in China, and the resulting decrease in emissions, have caused a reduction in concentrations of air pollutants measured by ground and satellite observations in East Asia (Forster *et al* 2020, Le *et al* 2020, NASA 2020, Shi and Brasseur 2020, Wang *et al* 2020a), the atmospheric CO_2 levels across various locations in East Asia reached their highest levels in 2020 (figure 1): e.g. Anmyeondo (AMY) in South Korea, Minamitorishima (MNM) in Japan, and Mt Waliguan (WLG) in China. It was expected that the dramatic decrease of local emission across East Asia would reduce the atmospheric CO_2 measured at local stations; however, such a phenomenon was not observed due to the challenging nature of signal detection for CO_2 observation. First, CO_2 is a long-lived gas; thus, even if emissions are reduced for a few weeks, the background levels remain unchanged (Friedlingstein *et al* 2020). Second, the signal of reduced CO_2 emissions is small compared to the monthly CO_2 uptake and release by terrestrial ecosystems (Peters *et al* 2017, Le Quéré *et al* 2020). Third, atmospheric transport is rapid in the Northern Hemisphere and quickly mixes the emission signal with terrestrial and oceanic fluxes on time scales of a few days to weeks, where strong synoptic CO_2 variations are driven by meteorological conditions (Ballantyne *et al* 2012, Peters *et al* 2017, Le Quéré *et al* 2020). To overcome these challenges, it is necessary to isolate the recent change in CO_2 mole fractions above the background level, to exclude the influence of the terrestrial ecosystem, and to minimize the mixing effect of atmospheric transport.

This study investigates whether the emission decrease in China due to COVID-19 was detected in the CO_2 and CO levels measured at the AMY global atmosphere watch (GAW) station, located on the west coast of South Korea, downwind of China. In addition to the regional fluxes of South Korea, these measurements are affected by Northeast Asian fluxes, including those in China (Yun *et al* 2020). Although lockdown in China lasted until April 2020, we focused the period from February to March 2020, when the impact of the terrestrial ecosystem might be neglected due to vegetation dormancy (Piao *et al* 2006) and CO_2 emissions in China decreased dramatically by 14% (Liu *et al* 2020). Our data were divided into two time periods: (a) the LOCK period (lockdown period in China, February to March 2020), and (b) the REF period (reference period, February to March 2018 and 2019). Data obtained during the LOCK period were compared with those obtained during the REF period. Because the CO_2 and CO levels measured at AMY are affected by a mixture of carbon emissions from several regions owing to atmospheric transport, we used the Weather Research and Forecasting–Stochastic Time-Inverted Lagrangian Transport (WRF-STILT) model to classify the air parcels from China.

2. Methods

2.1. ΔCO_2 and ΔCO levels at AMY

The AMY station (36° 32 19″ N, 126° 19 48″ E, and 47 m asl), as a regional station under the GAW programme of the World Meteorological Organization, monitors atmospheric greenhouse gases and air pollutants in South Korea (figure 1(a)). The station is operated by the Korea Meteorological Administration/National Institute of Meteorological Sciences. It has continuously recorded CO_2 and CO levels since 1999 and 2004, respectively (Zellweger *et al* 2019). A cavity ring-down spectroscopy analyzer (model G2301, Picarro, CA, USA) continuously monitors atmospheric CO_2; the measurement uncertainty is within 0.116 ppm in the 68% confidence interval (Lee *et al* 2019). The CO analyzer (model 48i, Thermo Fisher, MA, USA), based on non-dispersive infrared (NDIR) technology, has an uncertainty within 29.076 ppb in the 68% confidence interval (Zellweger *et al* 2019).

Because CO_2 and CO remain in the atmosphere for at least 300 years and 2 months, respectively (Khalil and Rasmussen 1990, Buis 2019), the measured CO_2 and CO mole fractions can be attributed to two factors: the recent enhancement and long-maintained background level. To capture the increase above the background level, i.e. enhancement from recent anthropogenic emissions, it is necessary to remove background levels for CO_2 and CO. The MNM station (24° 17′ 18″ N, 153° 58′ 60″ E, and 7.1 m asl) was chosen as the background atmospheric station to obtain the enhancements in CO_2 (ΔCO_2) and CO (ΔCO) above the background. An NDIR analyzer (model LI-7000, LI-COR Biosciences, Inc., NE, USA) and gas chromatography (reduction gas detector) analyzer (TRA-1, Round Science Inc., Kyoto, Japan) were used to monitor the CO_2 and CO levels at MNM, respectively. In addition, we applied the WLG flask data (Dlugokencky *et al* 2020, Petron *et al* 2020) to calculate ΔCO_2 and ΔCO, and there were no significant differences in the main findings (see supplementary note 1 available online at stacks.iop.org/ERL/17/024036/mmedia WLG background station). The WLG station was not used as the main background station in this study, as it provides flask-sampled data and the amount of data during the analysis period is small. The choice of background did not lead to significant changes in our

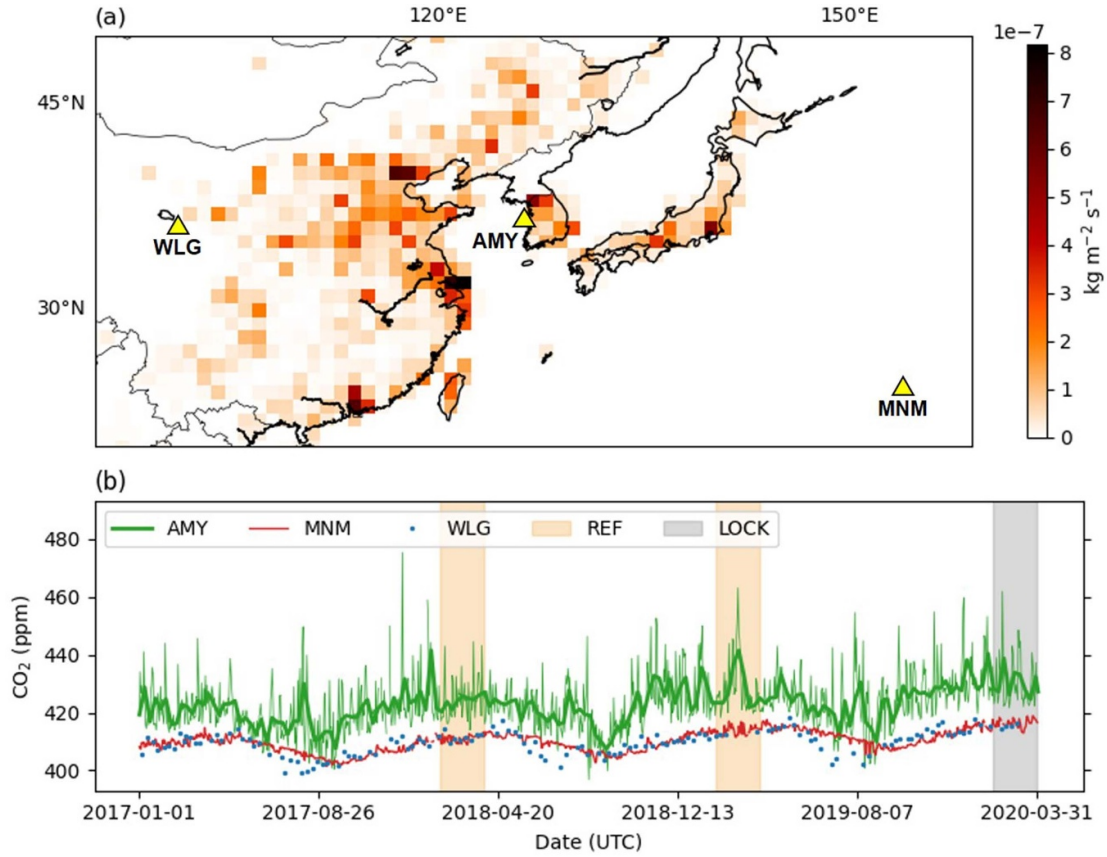

Figure 1. The spatiotemporal characteristics of CO_2 in East Asia. (a) Map of fossil fuel CO_2 emissions from Open-source Data Inventory for Anthropogenic CO_2 in February 2019 (Oda and Maksyutov 2011) and locations of WLG, AMY, and MNM stations. (b) Time series of CO_2 levels measured at AMY, MNM, and WLG from 2017 to 2020. Data that were regarded as background data were used for MNM and WLG. Lines for AMY and MNM indicate daily-averaged data from hourly data and thick line for AMY indicates weekly-averaged data. Dots for WLG indicate day-to-day sparsely sampled flask data. Orange and gray shaded regions indicate REF (February to March 2018 and 2019) and LOCK periods (February to March 2020), respectively.

results because the enhancement in AMY is largely affected by regional and local signals (Turnbull *et al* 2011b, Lee *et al* 2020).

Various steps were undertaken to calculate hourly ΔCO_2 and ΔCO values at AMY (figure 2). First, values considered as the background were used from the hourly data provided by MNM because they are not affected by local sources and sinks. The filtered hourly MNM data were averaged to daily data in order to apply the background level condition identically to the flask-sampled WLG data, which have no continuous hourly data. We interpolated the daily CO_2 data at MNM from a curve fit (Thoning and Tans 1989, Turnbull *et al* 2011a, NOAA 2021), thereby filling the background values for days that have been filtered or not observed due to other problems. For CO data at MNM, linear interpolation was applied to fill the empty daily data. The hourly ΔCO_2 and ΔCO values at AMY were then calculated by subtracting the interpolated daily MNM data from the hourly AMY data observed on the same date (e.g. hourly $\Delta CO_2{}^{AMY}$ = hourly $CO_2{}^{AMY}$ − interpolated daily $CO_2{}^{MNM}$ and hourly ΔCO^{AMY} = hourly CO^{AMY} − interpolated daily CO^{MNM}).

2.2. WRF-STILT experiments

WRF model version 3.9.1 (Skamarock and Klemp 2008) was used to generate meteorological fields to drive the STILT model (Lin *et al* 2003); the grid spacing was 27 km (103° E–138° E and 20° N–51° N) (see supplementary note 2 WRF configuration). Reanalysis data from the Global Forecast System produced by the National Centers for Environmental Prediction were applied as boundary conditions to the WRF model at a horizontal resolution of 0.5° every 6 h.

The STILT model, driven by meteorological fields simulated by the WRF model, was utilized to determine when the observed mole fractions at AMY were affected by China. WRF-STILT is an effective tool for simulating realistic atmospheric transport using the Lagrangian particle dispersion model within the planetary boundary layer (Nehrkorn *et al* 2010). It releases backward 3D air parcel trajectories with stochastically turbulent dispersion from the observation location (receptor) to a potential source region that affects the receptor and counts the scattered air parcels (footprints) in each grid. As defined in equations (7) and (8) by Lin *et al*

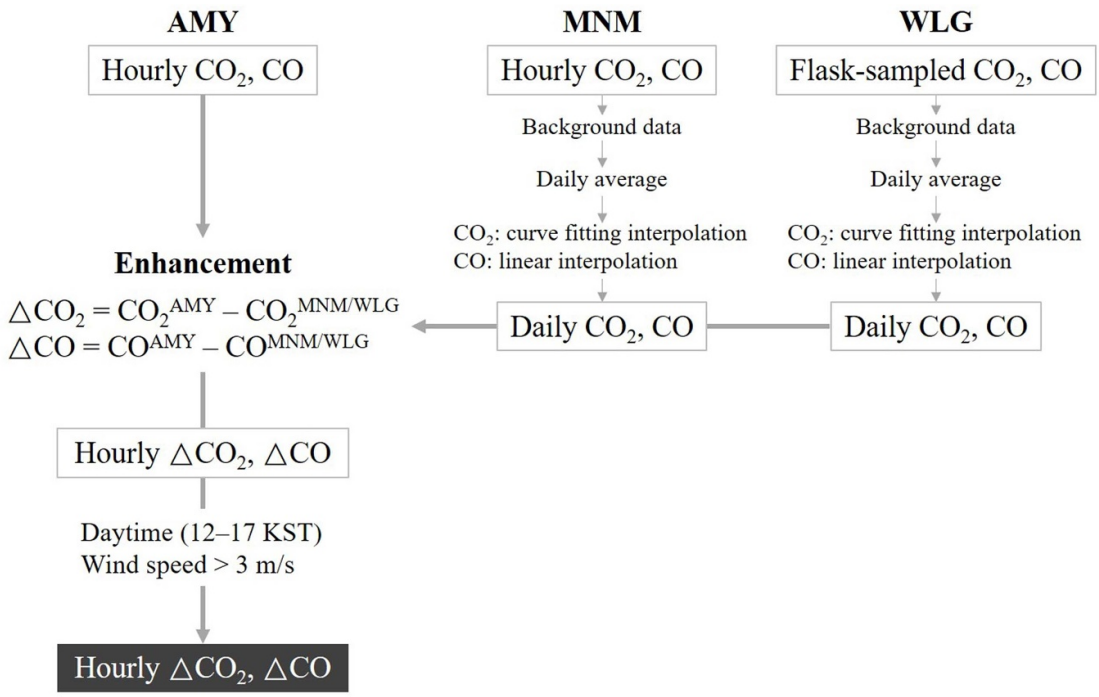

Figure 2. The workflow of the data processing of CO_2 and CO observations measured by AMY, MNM, and WLG to calculate enhancements values with applying the non-stagnant conditions.

(2003), footprints quantify the sensitivity of observation to upstream source regions. Footprints can be regarded as the average contribution of the surface flux at the receptor, as they represent how dense and how long the particle parcels lingered backward in time in each discretized volume in the upwind source regions. Therefore, in this study, areas with higher footprint values were considered to be the main source regions, which heavily affected the observed ΔCO_2 and ΔCO at AMY. Three hundred air parcels were released within WRF-STILT and tracked backward in time from AMY for 48 h (supplementary figure 1).

2.3. Source region separation

According to Lee *et al* (2019), the measured atmospheric gases at AMY are sensitive to emissions from China, depending on the wind speed and direction. Therefore, in this study, we need to consider wind and footprint with adequate conditions to capture the impact of Chinese emissions. According to the conditions used by Yun *et al* (2020), only the daytime observations (12:00–17:00 KST) with wind speeds above 3 m s^{-1} were used to minimize the effect of local emission sources because these are most likely to influence AMY observations under stagnant conditions (figure 2).

To determine source origin, footprints for the preceding 48 h simulated by WRF-STILT were used. The footprints for the backward 48 h that affected the observed mole fractions at AMY were calculated for each grid cell with 48 time steps (−1, −2, …, −48 h). The footprints of the 48 simulated time steps were averaged to create an average footprint map for every hour. The sum of footprints for each country was calculated by adding the footprint values for each grid located within the country boundaries of China, South Korea, and North Korea (figure 3(a)). If the sum of the footprints within the Chinese border at each time was greater than twice the sum of footprints in South Korea and North Korea, the air parcels brought into AMY were classified as being of Chinese origin. Moreover, when the air parcels originated from China, the majority of the WRF-STILT footprint results could be classified as originating from East China and Northeast China (figures 3(b) and (c)). Among air parcels of Chinese origin, if the sum of the footprints at the East China boundary was greater than twice that within the Northeast China boundary, it was classified as originating from East China, with the opposite being true for those originating from Northeast China.

2.4. Statistical methods

A Welch's *t*-test was used to determine the significant difference between the means of the two sampled data during the REF and LOCK periods (Welch 1947). The *t*-test requires that each sample is insensitive to autocorrelation, otherwise the *t*-test is less stringent (Ebisuzaki 1997, Wilks 1997). Because there were autocorrelations in hourly ΔCO_2 and ΔCO during the REF and LOCK periods, we averaged

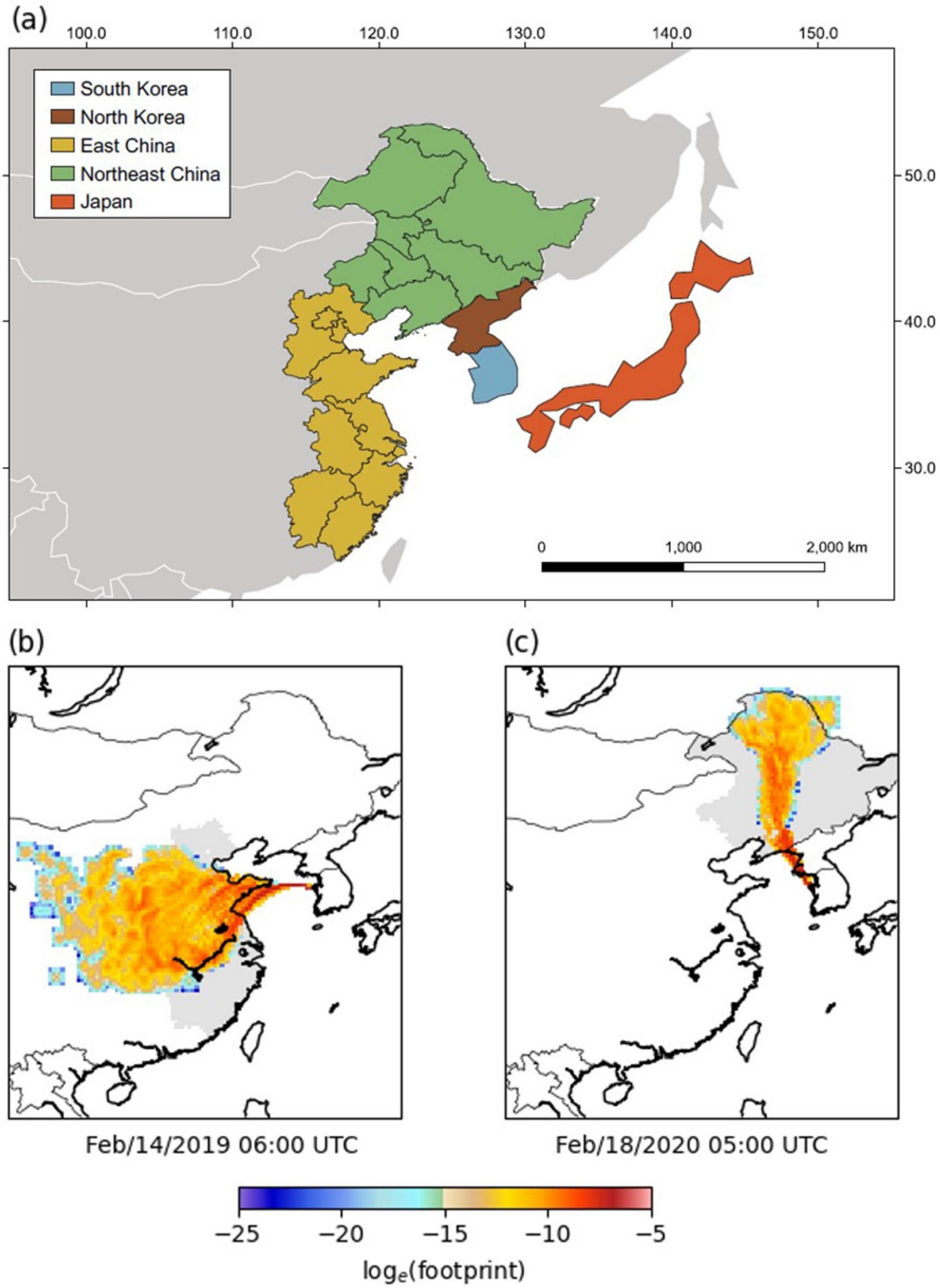

Figure 3. (a) Map of East Asia with each spatial area for South Korea, North Korea, East China, and Northeast China for separating source origins. Each map shows the typical source origins from (b) East China and (c) Northeast China. Averaged footprints derived from particle locations generated by WRF-STILT model −48 h upstream of AMY station. Gray shaded regions indicate the ranges of East China and Northeast China. East China includes Beijing, Tianjin, Shanghai, Jiangsu, Zhejiang, Anhui, Fujian, Jiangxi, Shandong, and Hebei. Northeast China includes Liaoning, Jilin, Heilongjiang, and some prefecture-level units in Inner Mongolia Autonomous Region (Chifeng, Hinggan League, Hulunbuir, and Tongliao).

hourly ΔCO_2 (or ΔCO) on the same day into daily data to remove the autocorrelation (Ebisuzaki 1997, Wang *et al* 2013). Averaging hourly ΔCO_2 and ΔCO data to daily data resulted that each data had no autocorrelation. Also, we used 95% confidence intervals to express plausible ranges for the sample means, and all ranges reported via ± are the 95% confidence intervals of the mean.

3. Results

3.1. Changes in ΔCO_2 and ΔCO during lockdown period

The atmospheric CO_2 levels measured at AMY, MNM, and WLG show seasonal variability and continue to increase over time (figure 1(b)). The CO_2 growth rates from 2017 to 2020 were 2.94, 1.92, and 1.82 ppm year^{-1} at AMY, MNM, and WLG, respectively. Compared to background stations (410.21 $\pm$ 0.2 ppm at MNM and 409.73 $\pm$ 0.23 ppm at WLG), AMY had higher mean values with higher variations (422.95 $\pm$ 0.54 ppm). All error ranges in the results indicate a 95% confidence interval on the mean. CO_2 levels measured at AMY include the effect from surrounding countries in addition to those from the local region, therefore, it was somewhat difficult to differentiate the differences in ΔCO_2 and ΔCO due to the COVID-19 lockdown in China from noise.

To focus on the effect of lockdown in China, ΔCO_2 and ΔCO in air parcels from China during the lockdown were compared with values from the same period in the previous 2 years (figure 4). Figure 4(a) shows the time series of all data of ΔCO_2 and ΔCO measured at AMY during the REF and LOCK periods, regardless of the inflow path of air parcels. The average ΔCO_2 during LOCK (13.9 $\pm$ 0.5 ppm) was similar to that during the REF period (14.1 $\pm$ 0.4 ppm). ΔCO_2 did not decrease during the LOCK period compared to the REF period, despite the COVID-19 lockdown. Unlike ΔCO_2, the average ΔCO during the LOCK period (168.8 $\pm$ 6.2 ppb) was lower than that during the REF period (231.8 $\pm$ 6.4 ppb).

Triangles in figure 4(a) shows the cases for air parcels originating from China classified based on the WRF-STILT modeling results. Using these cases, the average ΔCO_2 and ΔCO during the REF and LOCK periods were compared, and the monthly differences were analyzed (figure 4(b)). Air parcels from China had lower ΔCO_2 and ΔCO during the LOCK period compared to that during the REF period. The averaged ΔCO_2 values during the REF and LOCK periods were 9.46 $\pm$ 1.02 ppm and 7.54 $\pm$ 0.72 ppm, respectively. The averaged ΔCO_2 during the LOCK period decreased by -1.92 ppm (-20%) relative to that during the REF period. As for monthly differences, although ΔCO_2 slightly reduced in February when comparing the REF period with the LOCK period, that in March during the LOCK period significantly decreased by -3.61 ppm (-34%), beyond the 95% confidence intervals. The ΔCO decreased by -80.66 ppb (-43%) during the LOCK period compared to that during the REF period, and the reduction was more pronounced in March (-51%) than that in February (-36%). The results obtained using WLG flask data as a reference were consistent with those obtained using MNM data. The WLG results had lower ΔCO_2 and ΔCO values during the LOCK period relative to the REF period, and the differences between REF and LOCK periods were relatively small in February and significantly greater in March (see supplementary note 1).

The result from daily-averaged ΔCO_2 and ΔCO (no autocorrelation) between the REF and LOCK periods in supplementary figure 2 had no significant differences in the main findings in figure 4(b). The daily-averaged ΔCO_2 values during the REF and LOCK periods were 10.15 $\pm$ 2.17 ppm and 7.43 $\pm$ 1.08 ppm, respectively (supplementary figure 2). For daily-averaged ΔCO, their mean values showed 203 $\pm$ 56.8 ppb and 98.5 $\pm$ 28.4 ppb during the REF and LOCK periods, respectively. Two-sided t-tests showed that the differences in both daily-averaged ΔCO_2 and ΔCO between the REF and LOCK periods were statistically significant ($\alpha = 0.05$). The p-values obtained for ΔCO_2 and ΔCO were 0.029 and 0.002 between REF and LOCK periods, respectively. Although ΔCO_2 in February did not show a statistically significant difference ($p > 0.05$), both ΔCO_2 and ΔCO significantly decreased in March during the LOCK period ($p < 0.05$).

The changes in ΔCO_2 and ΔCO responses to COVID-19 in February and March could be influenced by meteorology. North China, including Beijing, experienced air stagnation caused by decreased wind speed and declined PBL height during the city lockdown from 23 January to 13 February 2020 (Le *et al* 2020). Air stagnation in China may explain the greater decrease in ΔCO_2 and ΔCO in March compared to those in February 2020, when the emission decrease was larger. The asymmetric changes between the 2 months are consistent with the satellite data results. The monthly average ΔCO in Beijing in 2020 was 6.3% and 18.0% lower in February and March, respectively, compared to that in 2019 (Cai *et al* 2021). The similarity between our results and those of previous studies confirms that the effect of emission reductions from China due to COVID-19 could be detected through atmospheric observations at AMY.

3.2. Changes in ΔCO_2 and ΔCO in air parcels from different Chinese source regions

There are significant differences in emission characteristics within China, depending on the region. East China has more major cities, including Beijing, Tianjin, and Shanghai, and industries than Northeast China. East China's GDP was three times higher on average than that of Northeast China in 2019 (Statista 2021). To compare and contrast the changes in ΔCO_2 and ΔCO at AMY depending on regional differences in emission characteristics, cases which were influenced by surface fluxes in China are separated

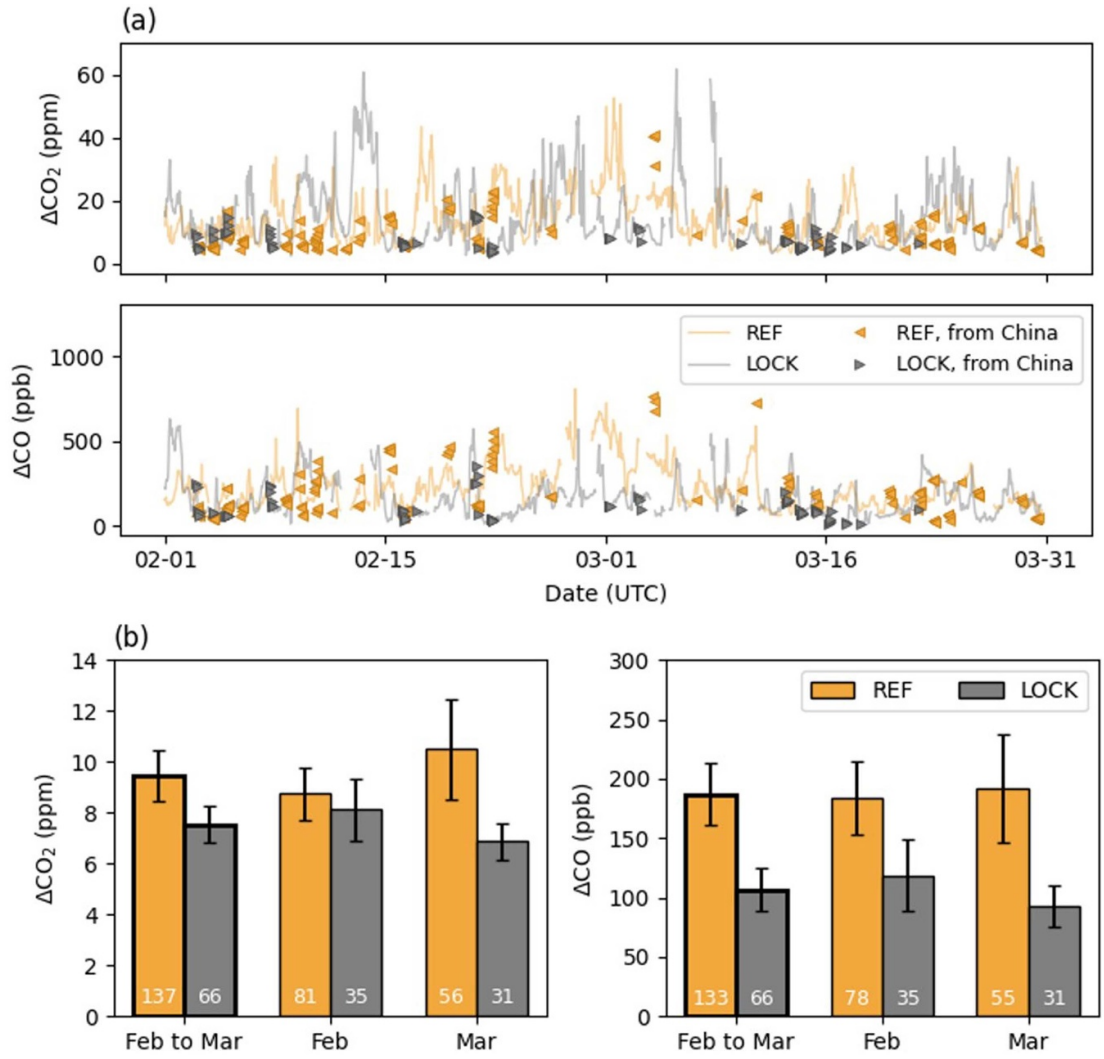

Figure 4. Comparison of ΔCO_2 and ΔCO between the REF and LOCK periods. (a) Time series of ΔCO_2 (top) and ΔCO (bottom) from February to March for 2018–2020. Orange lines and triangles are ΔCO_2 (ΔCO) values for averaged data from 2018 and 2019, and for air parcels originating from China during the REF period (February to March 2018 and 2019), respectively. Gray lines and triangles are ΔCO_2 (ΔCO) values for all data, and for air parcels originating from China during the LOCK period (February to March 2020), respectively. (b) ΔCO_2 (left) and ΔCO (right) during REF and LOCK periods for air parcels originating from China. The error bars indicate the 95% confidence intervals on the mean of the population. The white numbers in bars indicate the number of data used.

into two different regions: East China and Northeast China (figure 3). Data where air parcels were found to be of Chinese origin but were not classified as being from the East or Northeast China were excluded from this analysis.

Figure 5 shows the average ΔCO_2 and ΔCO values for air parcels originating from East China and Northeast China during the REF and LOCK periods. The number of affected samples from Northeast China, compared to that from East China, was 1.5 times more during the REF period and three times more during the LOCK period. On average, during the REF period, ΔCO_2 was higher for East China (11.9 ± 2.3 ppm) than that for Northeast China (7.7 ± 0.7 ppm). During the REF period, ΔCO had a higher value when air parcels originated from East China than from Northeast China (241.5 ± 51 ppb for East China and 150.9 ± 27.5 ppb for Northeast China). The higher ΔCO_2 and ΔCO in air parcels originating from East China during the REF period can be attributed to higher emissions from this area, which has more than three times the carbon emissions of Northeast China. According to national statistics for Chinese provinces, estimated carbon emissions were 3857.93 Mt CO_2 for East China and 1085.5 Mt CO_2 for Northeast China in 2017 (Shan *et al* 2020).

When compared to that during the REF period, the average ΔCO_2 during the LOCK period decreased when originating from East China (6.6 ± 0.9 ppm) but did not decrease when originating from Northeast China (7.7 ± 0.9 ppm). Compared to the REF period, ΔCO during the LOCK period decreased regardless of the source region, as 85.4 ± 29.5 ppb for East

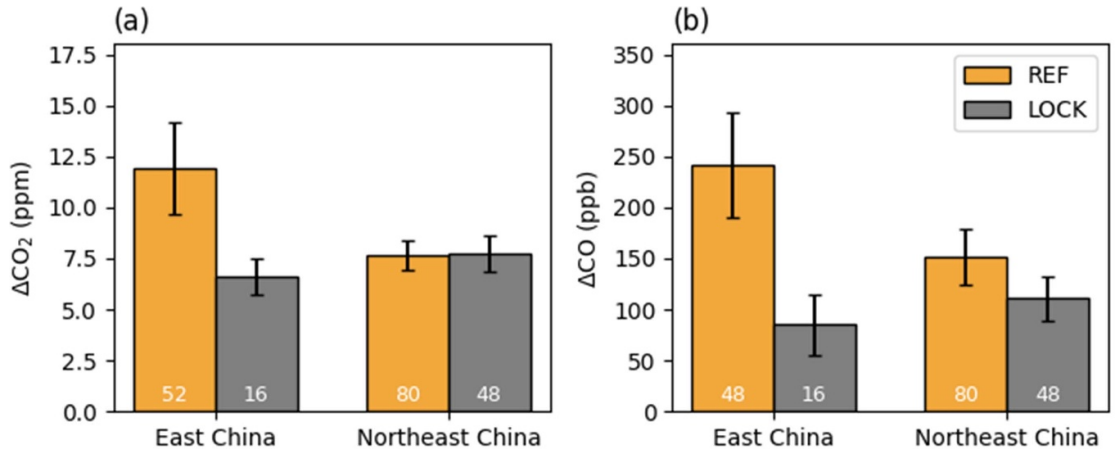

Figure 5. Changes in ΔCO_2 and ΔCO in air parcels from different source regions during the lockdown in China and the same period in previous years. Averaged (a) ΔCO_2 and (b) ΔCO in air parcels originating from East China and Northeast China during the REF and LOCK periods. The error bars indicate the 95% confidence intervals on the mean of the population. The white numbers in bars indicate the number of data used.

China and 110.7 ± 21.9 ppb for Northeast China. The reduction rate between REF and LOCK periods was more dominant when the air parcels originated from East China for both ΔCO_2 and ΔCO. For East China, the reduction rates in ΔCO_2 and ΔCO were approximately −44% and −65%, respectively. The East China reductions are beyond the 95% confidence intervals and statistically significant from the two-sided *t*-test ($p < 0.05$). The changes in ΔCO_2 and ΔCO for Northeast China were +1% ($p > 0.05$) and −27% ($p > 0.05$), respectively.

The results presented here (figure 5) are in agreement with previous studies, which observed noticeable decreases in pollutant concentrations (NO_2, $PM_{2.5}$, and CO) in East China, which includes the North China Plain, compared to Northeast China, according to *in situ* data obtained within China or satellite data (Huang and Sun 2020, Wang *et al* 2020b, Hammer *et al* 2021). East China, which is economically active and carbon-intensive, was more affected by the COVID-19 lockdown than Northeast China, resulting in similar ΔCO_2 and ΔCO between the two regions during the LOCK period. Though it has not been extensively reported in recent China-focused studies, these results suggest that each region in China may have a different atmospheric CO_2 reduction due to COVID-19.

3.3. Changes in emission characteristics due to lockdown

The $\Delta CO/\Delta CO_2$ ratio refers to the proportion of emitted CO relative to emitted CO_2 from the same anthropogenic combustion sources. It can be used to distinguish the source region/type and for estimating the combustion efficiency (Suntharalingam *et al* 2004, Wang *et al* 2010, Turnbull *et al* 2011a, Tohjima *et al* 2014, Niu *et al* 2018, Tang *et al* 2018, Lee *et al* 2020, Sim *et al* 2020). A higher $\Delta CO/\Delta CO_2$ ratio indicates that the source regions have incomplete combustion, and that most of the source types are domestic coal and biofuel combustion, with low contributions of vehicles with catalytic converters. The $\Delta CO/\Delta CO_2$ ratio comparison for air parcels from China and South Korea during the REF period was conducted as per supplementary note 3. The ratio for China was twice that of South Korea because of their use of biomass and domestic coal which emit more CO and have relatively low combustion efficiency. When compared with the $\Delta CO/\Delta CO_2$ ratios determined in previous studies, the ratio found in the present study for China was lower due to improvements in combustion efficiency and strict CO emission controls in recent years.

To investigate the changes in emission characteristics in China due to COVID-19, the ratios of ΔCO to ΔCO_2 between REF and LOCK periods were compared (figure 6). The $\Delta CO/\Delta CO_2$ ratio indicates the slope of the reduced major axis regression between ΔCO_2 and ΔCO. The $\Delta CO/\Delta CO_2$ ratios were 24.81 ± 0.88 ppb ppm^{-1} ($r = 0.92$) and 24.75 ± 2.5 ppb ppm^{-1} ($r = 0.67$) during the REF and LOCK periods, respectively, and the difference in ratios was not significant ($p > 0.05$). This suggests that emission characteristics, such as emission sources and combustion efficiency, might not change despite the significant decrease in ΔCO_2 and ΔCO during the LOCK period. That is, the significant decrease in in ΔCO_2 and ΔCO during the LOCK period is due to the effect of the reduction of emissions due to COVID-19. The reduction in the high enhancement cases for both ΔCO_2 and ΔCO during the LOCK period (figure 6) also supports this implication.

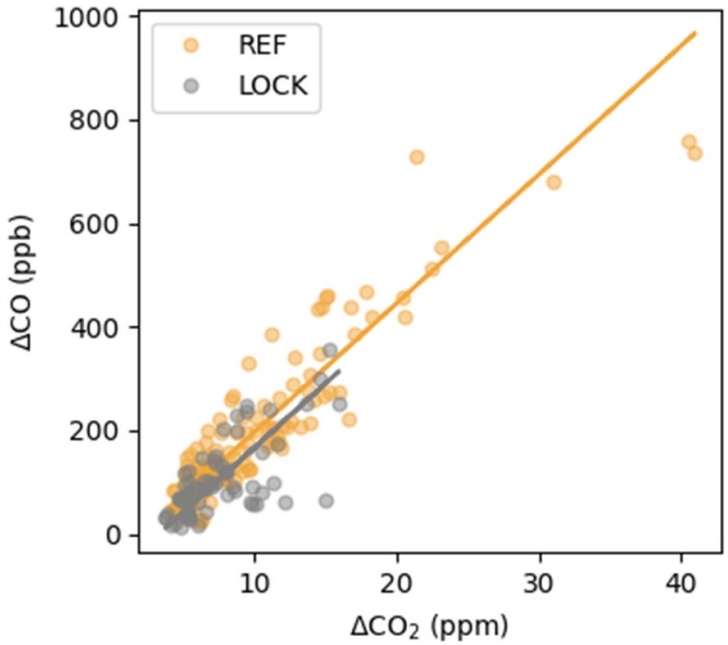

Figure 6. Linear regressions between ΔCO_2 and ΔCO when AMY observations were affected by air parcels from China for REF (orange color) and LOCK (gray color) periods. There are 133 and 66 data points for the REF and LOCK periods, respectively.

4. Discussion and conclusion

Due to social restrictions during the first COVID-19 pandemic period in 2020, CO_2 emissions in China sharply decreased, leading to expectations that the atmospheric CO_2 level can be diminished. However, studies using satellite data to measure column-averaged dry-air mole fractions of CO_2 have failed to detect any significant reductions (Chevallier *et al* 2020, Sussmann and Rettinger 2020, Buchwitz *et al* 2021, Cai *et al* 2021). Instead, only ground-based observations near South China have found a significant reduction in the $\Delta CO_2/\Delta CH_4$ ratios (Tohjima *et al* 2020). Although there have been several attempts to determine the decrease in atmospheric CO_2 levels due to COVID-19, the rapid atmospheric mixing in the Northern Hemisphere dilutes the signal with the 'noise', making it difficult to detect the signal of reduced emissions.

Despite these difficulties, the present study detected a significant reduction in the short-term regional enhancement of the observed atmospheric CO_2 during the first COVID-19 pandemic period in 2020. We were able to verify the impact of the entire Chinese continent by using observations at a regional monitoring station in South Korea, an area downwind of China. Because the CO_2 background levels continued to increase, CO_2 enhancements above the background level were used to capture the changes from recent anthropogenic emissions during the COVID-19 lockdown. The WRF-STILT model was then applied to isolate the influence of China while minimizing the effect of rapid atmospheric transport in the Northern Hemisphere. The $\Delta CO/\Delta CO_2$ ratio was utilized to identify changes in China's emission characteristics due to COVID-19. Although vegetation activity and soil respiration in winter might have negligible effects on the variation in CO_2 levels, further studies using process-based models are needed to evaluate the possible effects of vegetation activity and soil respiration on the observed CO_2 variations.

When affected by air parcels from China, ΔCO_2 decreased on average by -1.92 ± 0.03 ppm in 2020, particularly by -3.61 ± 0.06 ppm in March, compared to the same period in 2018 and 2019. According to Tohjima *et al* (2020), a 10% global CO_2 emissions reduction results in approximately a -0.5 ppm decrease in atmospheric CO_2. The estimated reductions in CO_2 emissions in China from previous studies were -18.4% and -9.2% in February and March 2020, respectively (Liu *et al* 2020). The reason why the atmospheric ΔCO_2 reduction in this study is a large response to the emission reduction may be because this study targets China, which experienced the greatest emission reductions worldwide. The ΔCO_2 decreased sharply in East China compared to Northeast China, indicating that the eastern region had a significant impact on ΔCO_2 in China. These results were similar when using MNM or WLG as the background station because the enhancement of AMY is heavily influenced by regional and local signal.

Although the average global atmospheric CO_2 level is still increasing, this study revealed the atmospheric impact of COVID-19 lockdown-induced carbon emission reductions in China, suggesting that the CO_2 level might decrease or increase at a much slower rate if substantial emission reductions are achieved

in multiple nations. The reduction of human activity to address the COVID-19 pandemic clearly illustrates how the increase in atmospheric CO_2 levels can be controlled, which is a major factor in directly mitigating climate change.

Data availability statement

The data that support the findings of this study are available upon reasonable request from the authors.

Acknowledgments

We are grateful to WMO World Data Center for Greenhouse Gases (WMO/WDCGG, http://gaw.kishou.go.jp/wdcgg.html) operated by Japan Meteorological Agency (JMA) for providing data at MNM station. We also acknowledge WLG station in China and Mauna Loa station in Hawaii for their data contributions. This work was funded by the Korea Meteorological Administration Research and Development Program "Development of Monitoring and Analysis Techniques for Atmospheric Composition in Korea" under Grant (KMA2018-00522).

Conflict of interest

The authors declare no conflicts of interest.

ORCID iDs

Sojung Sim https://orcid.org/0000-0003-4948-0941
Philippe Ciais https://orcid.org/0000-0001-8560-4943
Shilong Piao https://orcid.org/0000-0001-8057-2292
Hoonyoung Park https://orcid.org/0000-0002-7856-5218
Sujong Jeong https://orcid.org/0000-0003-4586-4534

References

Ballantyne A P, Alden C B, Miller J B, Trans P P and White J W C 2012 Increase in observed net carbon dioxide uptake by land and oceans during the past 50 years *Nature* **488** 70–73

Buchwitz M *et al* 2021 Can a regional-scale reduction of atmospheric CO_2 during the COVID-19 pandemic be detected from space? A case study for East China using satellite XCO_2 retrievals *Atmos. Meas. Tech.* **14** 2141–66

Buis A 2019 The atmosphere: getting a handle on carbon dioxide (NASA's Jet Propuls. Lab) (available at: https://climate.nasa.gov/news/2915/the-atmosphere-getting-a-handle-on-carbon-dioxide/)

Cai Z, Che K, Liu Y, Yang D, Liu C and Yue X 2021 Decreased anthropogenic CO_2 emissions during the COVID-19 pandemic estimated from FTS and MAX-DOAS measurements at urban beijing *Remote Sens.* **13** 1–12

Chevallier F, Zheng B, Broquet G, Ciais P, Liu Z, Davis S J, Deng Z, Wang Y, Bréon F-M and O'Dell C W 2020 Local anomalies in the column-averaged dry air mole fractions of carbon dioxide across the globe during the first months of the coronavirus recession *Geophys. Res. Lett.* **47**

Dlugokencky E J, Mund J W, Crotwell A M, Crotwell M J and Thoning K W 2020 Atmospheric carbon dioxide dry air mole fractions from the NOAA GML carbon cycle cooperative global air sampling network, 1968–2019 Version: 2020–07 (https://doi.org/10.15138/wkgj-f215)

Ebisuzaki W 1997 A method to estimate the statistical significance of a correlation when the data are serially correlated *J. Clim.* **10** 2147–53

Forster P M *et al* 2020 Current and future global climate impacts resulting from COVID-19 *Nat. Clim. Change* **10**

Friedlingstein P, Sullivan M O, Jones M W, Andrew R M and Hauck J 2020 Global carbon budget 2020 *Earth Syst. Sci. Data* **12** 3269–340

Hammer M S *et al* 2021 Effects of COVID-19 lockdowns on fine particulate matter concentrations *Sci. Adv.* **7** eabg7670

Huang G and Sun K 2020 Non-negligible impacts of clean air regulations on the reduction of tropospheric NO_2 over East China during the COVID-19 pandemic observed by OMI and TROPOMI *Sci. Total Environ.* **745** 141023

Khalil M A K and Rasmussen R A 1990 The global cycle of carbon monoxide: trends and mass balance *Chemosphere* **20** 227–42

Le Quéré C *et al* 2020 Temporary reduction in daily global CO_2 emissions during the COVID-19 forced confinement *Nat. Clim. Change* **10** 647–53

Le T, Wang Y, Liu L, Yang J, Yung Y L, Li G and Seinfeld J H 2020 Unexpected air pollution with marked emission reductions during the COVID-19 outbreak in China *Science* **369** 702–6

Lee H *et al* 2020 Observations of atmospheric $14CO_2$ at Anmyeondo GAW station, South Korea: implications for fossil fuel CO_2 and emission ratios *Atmos. Chem. Phys.* **20** 12033–45

Lee H, Han S-O, Ryoo S-B, Lee J and Lee G 2019 The measurement of atmospheric CO_2 at KMA/GAW regional stations, the characteristics, and comparisons with other East Asian sites *Atmos. Chem. Phys.* **19** 2149–63

Lin J C, Gerbig C, Wofsy S C, Andrews A E, Daube B C, Davis K J and Grainger C A 2003 A near-field tool for simulating the upstream influence of atmospheric observations: the stochastic time-inverted Lagrangian transport (STILT) model *J. Geophys. Res. Atmos.* **108**

Liu Z *et al* 2020 Near-real-time monitoring of global CO_2 emissions reveals the effects of the COVID-19 pandemic *Nat. Commun.* **11** 5172

Myllyvirta L 2020 Coronavirus temporarily reduced China's CO_2 emissions by a quarter (available at: www.carbonbrief.org/analysis-coronavirus-has-temporarily-reduced-chinas-co2-emissions-by-a-quarter)

NASA 2020 Airborne nitrogen dioxide plummets over China (available at: https://earthobservatory.nasa.gov/images/146362/airborne-nitrogen-dioxide-plummets-over-china)

Nehrkorn T, Eluszkiewicz J, Wofsy S C, Lin J C, Gerbig C, Longo M and Freitas S 2010 Coupled weather research and forecasting-stochastic time-inverted lagrangian transport (WRF-STILT) model *Meteorol. Atmos. Phys.* **107** 51–64

Niu Z, Zhou W, Feng X, Feng T, Wu S, Cheng P, Lu X, Du H, Xiong X and Fu Y 2018 Atmospheric fossil fuel CO_2 traced by $14CO_2$ and air quality index pollutant observations in Beijing and Xiamen, China *Environ. Sci. Pollut. Res.* **25** 17109–17

NOAA 2021 Curve fitting methods applied to time series in NOAA/ESRL/GMD (available at: https://gml.noaa.gov/ccgg/mbl/crvfit/crvfit.html)

Oda T and Maksyutov S 2011 A very high-resolution (1 km × 1 km) global fossil fuel CO_2 emission inventory derived using a point source database and satellite observations of nighttime lights *Atmos. Chem. Phys.* **11** 543–56

Peters G P *et al* 2017 Towards real-time verification of CO_2 emissions *Nat. Clim. Change* **7** 848–50

Petron G, Crotwell A M, Crotwell M J, Dlugokencky E, Madronich M, Moglia E, Neff D, Wolter S and Mund J W 2020 Atmospheric carbon monoxide dry air mole fractions from the NOAA GML carbon cycle cooperative global air sampling network, 1988–2020 Version: 2020–08 (https://doi.org/10.15138/33bv-s284)

Piao S, Fang J, Zhou L, Ciais P and Zhu B 2006 Variations in satellite-derived phenology in China's temperate vegetation *Glob. Change Biol.* **12** 672–85

Shan Y, Huang Q, Guan D and Hubacek K 2020 China CO_2 emission accounts 2016–2017 *Sci. Data* **7**

Shi X and Brasseur G P 2020 The response in air quality to the reduction of Chinese economic activities during the COVID-19 outbreak *Geophys. Res. Lett.* **47**

Sim S *et al* 2020 Co-benefit potential of urban CO_2 and air quality monitoring: a study on the first mobile campaign and building monitoring experiments in Seoul during the winter *Atmos. Pollut. Res.* **11** 1963–70

Skamarock W C and Klemp J B 2008 A time-split nonhydrostatic atmospheric model for weather research and forecasting applications *J. Comput. Phys.* **227** 3465–85

Statista 2021 Gross domestic product (GDP) of China in 2019, by region (available at: www.statista.com/statistics/278557/gdp-of-china-by-region/)

Suntharalingam P, Jacob D D, Palmer P I, Logan J A, Yantosca R M, Xiao Y, Evans M J, Streets D G, Vay S L and Sachse G W 2004 Improved quantificaion of Chinese carbon fluxes using CO_2/CO correlations in Asian outflow *J. Geophys. Res. Atmos.* **109** 1–13

Sussmann R and Rettinger M 2020 Can we measure a COVID-19-related slowdown in atmospheric CO_2 growth? Sensitivity of total carbon column observations *Remote Sens.* **12** 2387

Tang W *et al* 2018 Evaluating high-resolution forecasts of atmospheric CO and CO_2 from a global prediction system during KORUS-AQ field campaign *Atmos. Chem. Phys.* **18** 11007–30

Thoning K W and Tans P P 1989 Atmospheric carbon dioxide at Mauna Loa Observatory. 2. Analysis of the NOAA GMCC data, 1974–1985 *J. Geophys. Res.* **94** 8549–65

Tohjima Y, Kubo M, Minejima C, Mukai H, Tanimoto H, Ganshin A, Maksyutov S, Katsumata K, Machida T and Kita K 2014 Temporal changes in the emissions of CH_4 and CO from China estimated from CH_4/CO_2 and CO/CO_2 correlations observed at Hateruma Island *Atmos. Chem. Phys.* **14** 1663–77

Tohjima Y, Patra P K, Niwa Y, Mukai H, Sasakawa M and Machida T 2020 Detection of fossil-fuel CO_2 plummet in China due to COVID-19 by observation at Hateruma *Sci. Rep.* **10** 1–9

Turnbull J C, Tans P P, Lehman S J, Baker D, Conway T J, Chung Y S, Gregg J, Miller J B and Southon J R 2011a Atmospheric observations of carbon monoxide and fossil fuel CO_2 emissions from East Asia *J. Geophys. Res. Atmos.* **116** 1–14

Turnbull J C, Tans P P, Lehman S J, Baker D, Conway T J, Chung Y S, Gregg J, Miller J B, Southon J R and Zhou L X 2011b Atmospheric observations of carbon monoxide and fossil fuel CO_2 emissions from East Asia *J. Geophys. Res. Atmos.* **116** 1–14

Wang P, Chen K, Zhu S, Wang P and Zhang H 2020a Severe air pollution events not avoided by reduced anthropogenic activities during COVID-19 outbreak *Resour. Conserv. Recycl.* **158** 104814

Wang W, Ciais P, Nemani R R, Canadell J G, Piao S, Sitch S, White M A, Hashimoto H, Milesi C and Myneni R B 2013 Variations in atmospheric CO_2 growth rates coupled with tropical temperature *Proc. Natl Acad. Sci. USA* **110** 15163

Wang Y, Munger J W, Xu S, McElroy M B, Hao J, Nielsen C P and Ma H 2010 CO_2 and its correlation with CO at a rural site near Beijing: implications for combustion efficiency in China *Atmos. Chem. Phys.* **10** 8881–97

Wang Y, Yuan Y, Wang Q, Liu C G, Zhi Q and Cao J 2020b Changes in air quality related to the control of coronavirus in China: implications for traffic and industrial emissions *Sci. Total Environ.* **731** 139133

Welch A B L 1947 The generalization of 'student's' problem when several different population variances are involved published by: Oxford University Press on behalf of Biometrika Trust Stable *Biometrika* **34** 28–35

Wilks D S 1997 Resampling hypothesis tests for autocorrelated fields *J. Clim.* **10** 65–82

Yun J *et al* 2020 Enhanced regional terrestrial carbon uptake over Korea revealed by atmospheric CO_2 measurements from 1999 to 2017 *Glob. Change Biol.* **26** 3368–83

Zellweger C, Steinbacher M and Buchmann B 2019 System and performance audit of surface ozone, carbon monoxide, methane, and carbon dioxide at the regional gaw station Anmyeon-do Republic of Korea (available at: www.empa.ch/documents/56101/250799/Bukit_Koto_Tabang_2019.pdf/4a899e2b-9984-4948-a4d0-748781de84f5)